PassiveVLC: Enabling Practical Visible Light Backscatter Communication for Battery-free IoT Applications

Xieyang Xu[†], Yang Shen[†], Junrui Yang[♯], Chenren Xu[†], Guobin Shen[§], Guojun Chen[†], Yunzhe Ni[†*]

[†]Peking University [♯]Stanford University [§]Zepp Labs, Inc.
{xy.xu, sy2006, chenren, leochan, yunzhe.ni}@pku.edu.cn jackiey@stanford.edu jackyshen@zepplabs.com

ABSTRACT

This paper investigates the feasibility of practical backscatter communication using visible light for battery-free IoT applications. Based on the idea of modulating the light retroreflection with a commercial LCD shutter, we effectively synthesize these off-the-shelf optical components into a sub-*mW* low power visible light passive transmitter along with a retroreflecting uplink design dedicated for power constrained mobile/IoT devices. On top of that, we design, implement and evaluate PassiveVLC, a novel visible light backscatter communication system. PassiveVLC system enables a battery-free tag device to perform passive communication with the illuminating LEDs over the same light carrier and thus offers several favorable features including battery-free, sniff-proof, and biologically friendly for human-centric use cases. Experimental results from our prototyped system show that PassiveVLC is flexible with tag orientation, robust to ambient lighting conditions, and can achieve up to 1 *kbps* uplink speed. Link budget analysis and two proof-of-concept applications are developed to demonstrate PassiveVLC's efficacy and practicality.

CCS CONCEPTS

• **Hardware → Wireless devices**; • **Computer systems organization →** *Embedded systems*;

KEYWORDS

Visible Light Communication, Passive Communication, Backscatter, Battery-free, Internet of Things, Retroreflector

1 INTRODUCTION

The grand vision of Internet-of-Things (IoT) – bring everything to the Internet to better sense, understand and actuate the real world – is turning into reality at a quick pace. Indeed, most new generation of devices, ranging from externally powered home appliances [6, 32], mobile objects with large batteries [4], to miniature implantable sensors [42], thin and flexible wearables [15, 35], *etc.*, have claimed "IoT-capable". However, to fully realize the IoT vision, far larger amount of smart devices are yet to be deployed. Such devices are likely to be of small form factor, wireless communication and untethered when operating. Thus, energy consumption naturally becomes an obstacle. Analysis reveals that communication takes a significant portion of the overall energy consumption for typical IoT sensing devices. In consequence, how to enable extremely energy efficient wireless communication has become an active research front.

Recently, research efforts have shown that radio backscatter communication [23, 50] can effectively offer near zero-power (orders of μW) connectivity to small sensor devices and thus becomes a competitive communication paradigm in the IoT era. The major idea behind radio backscattering is to leverage existing infrastructures, such as TV band [31], FM radio [46] and WiFi channel [11, 22, 23, 49]. Along the line but exploring a different infrastructure – the lighting infrastructure, some previous work have demonstrated the possibility of backscattering the visible light for communications [28, 41].

Using light as the transmission medium, visible light communication (VLC) systems natively possess certain compelling merits, such as sniffing-proof and biological friendliness, over radio communication in human-centric applications. However, it is nontrivial to build a visible light backscatter system. Several issues need to be solved. First of all, in contrast to omni-directional radio propagation, the light is highly directional. While this property contributes to the favorable sniffing-proof feature, it requires precise mutual pointing between two communicating ends, which further demands the system to have accurate (relative) positioning capability and steerable optical components for proper alignment.

Secondly, unlike radio backscatter systems where the antenna coupling is highly efficient for their narrow specific spectrum band, the efficiency of optical coupling is typically very low (*e.g.* usually less than 20% via solar panels) as the visible light takes extremely wide spectrum. Direct optical coupling could neither harvest enough energy (*e.g.* hundreds of μW in indoor environments) to power up a high power LED (typically with hundreds of mW budget), nor its on/off state could effectively affect (hence directly modulate) the visible light transmission. Note that optical light concentrating components may help, but, again, it would require precise pointing and additional cost.

RetroVLC [28] solves these issues by exploiting the very nature of a retroreflector, *i.e.* reflecting the light back almost exactly along its incoming path, which not only achieves all-the-time precise pointing but also naturally concentrates the light energy for a point

*X.Xu, Y.Shen and J.Yang are the co-primary student authors. J.Yang was working on this project as part of his Bachelor thesis when he was with Peking University.

MobiCom '17, October 16–20, 2017, Snowbird, UT, USA

ACM ISBN 978-1-4503-4916-1/17/10…$15.00
https://doi.org/10.1145/3117811.3117843

light source. The prototyped system uses common retroflector fabrics and adopts On-off keying (OOK) communication for the uplink with a MCU-controlled LCD shutter, which however fundamentally limits the data rate – the fixed response time (*e.g.* a few milliseconds) of the commercial LCD when manufactured throttles its highest switching rate for OOK modulation. In addition, the nonlinear responses of LCD state to voltage changes makes it very difficult to produce precise multi-level signals, especially in the context of IoT devices. With these observations, the authors in [41] extended the idea of RetroVLC and resorted to use a plural of retroreflectors and LCD shutters to improve the data rate. A reflector and a LCD shutter form a 'pixel', each pixel can be switched on/off independently, and pulse amplitude modulation (PAM) is adopted to increase the rate in proportional to the number of pixels.

In this paper, we seek to improve the data rate of RetroVLC from the very heart of any communication system – the coding and modulation schemes. In particular, we make two key observations. Firstly, the Manchester coding used in RetroVLC is not optimized for bandwidth efficiency. Secondly, it is not necessary to "fully" switch on/off the LCD to convey a signal. When an LCD is charged or discharged, its transparency will change continuously and leads to a trend of increasing or decreasing signal strength at the receiver side. As long as this trend is distinguishable, we may stop the charing or discharging process early. Note that the distinguishability depends on the communication range and SNR, and should be set according to typical working range in practice. In addition, different LCD shutters may have different turn-over rate, but this observation remains valid as it is based on the intrinsic properties of LCD.

With these observations, we renovate the RetroVLC design with two major innovations: 1) We replace Manchester coding with Miller code, which doubles the bandwidth utilization and is still immune to the clock drift. This essentially yields 2x data rate improvement in theory; 2) We design a *trend-based* modulation and *code-assisted* demodulation scheme. This design effectively reduces the modulation time, hence directly translates to an increase in data rate. In our prototype, we managed to reduce the modulation time from 4 *ms* to 1 *ms*, which gives another 4x boost in data rate. It is nontrivial to achieve this change in demodulation as the dependencies between symbols and restrictions from coding scheme have to be taken into consideration. We formulate it as an optimization problem and solve it with dynamic programming. Note that the increased complexity solely happens at the reader side, and the tag (*i.e.* the IoT device) is not affected. As a remark, our innovation is orthogonal to that in [41] – the two can be combined to further improve the data rate.

In the following, we present the design, implementation and evaluation of PassiveVLC– a practical visible light backscatter communication subsystem for low-power IoT applications. We have prototyped PassiveVLC to demonstrate its practicality for deployments – the battery-free ViTag is approximately the size of a credit card and the ViReader could be organically integrated into normal LED-based illuminating infrastructure (*e.g.* flashlights or lamps), as shown in Fig. 1. We benchmarked our system under different ambient lighting conditions such as office environments, outdoor daytime/night and dark chamber. Experiments show that our ViTag prototype can achieve up to 1 *kbps* uplink speed, which is ~8x in practice speedup as compared to our implementation of RetroVLC, with a 120 ° flexible orientation under sub-*mW* power budget.

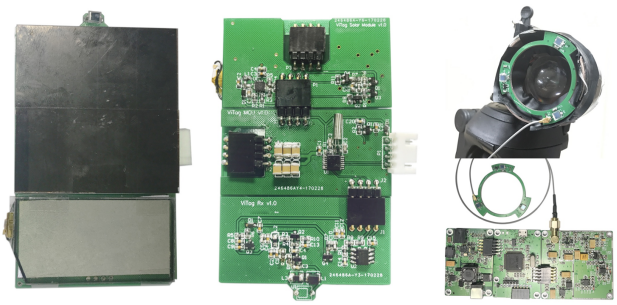

(a) ViTag Front (b) ViTag Back (c) ViReader

Figure 1: PassiveVLC system prototypes.

To better understand the design tradeoff (form factor, working range, *etc.*) among various components in PassiveVLC, based on the benchmark data, we derive and verify a joint link budget analysis for the downlink and uplink, which can serve as a guidance for developing PassiveVLC-enabled applications. Finally, we have built two proof-of-concept applications that illustrate the potential of PassiveVLC in real-world IoT applications. The first application is a smart check-in system where a ViReader-enabled door will automatically grant the access when a ViTag-bearing user walks into its working range. The second is an optical IoT networking solution where a ViReader-capable lighting LED infrastructure interrogates multiple ViTag-bearing IoT devices for streaming sensor readings.

Contributions.

- We design, implement and evaluate PassiveVLC, a practical visible light backscatter communication subsystem for battery-free IoT applications. With our optimized trend-based modulation and code-assisted demodulation design (§4), PassiveVLC achieves ~8x data rate improvement over the state-of-art (§5).
- We perform the joint link budget analysis (§6) for PassiveVLC's downlink and uplink, and experimentally verify the relationship between ViTag's form factor and desired communication range.
- We built two proof-of-concept applications for smart check-in system and optical IoT networks (§7) and demonstrated the practicality of PassiveVLC.

2 BACKGROUND

2.1 Design Considerations

PassiveVLC is essentially a two-way communication link using visible light, while fulfills the following two basic requirements:

- **Efficiency:** Operate under a low-power budget, *e.g.*, can work on a battery-free mobile/IoT end that harvests light energy from the illumination LED.
- **Practicality:** Impose as little constraints as possible on actual use. This implies a practical working range in normal indoor situations, flexible tag orientation, and small size of the device.

These requirements immediately exclude a symmetric design, *i.e.*, using a LED to establish the uplink to the reader because a practical working range would require a high power LED which is not quite

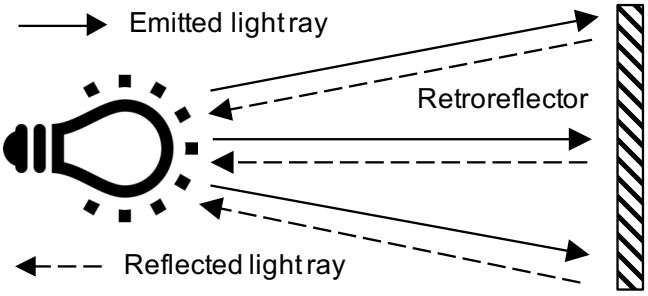

Figure 2: Energy concentrating property of a retroreflector when light source emits omni-directionally.

affordable by a small IoT device. It also excludes the adoption of optical light concentration component such as laser (to extend the working range) or mirror (to save the power for transmission power) as they would incur the overhead of precise pointing, a consequence of aforementioned directional propagation property of light. Inspired by free space laser communication systems [37], we use a *retroreflector* to meet both requirements.

2.2 Retroreflector and LCD Shutter

We introduce the principles and some (favorable) properties of the retroreflector and LCD.

2.2.1 Retroreflector As a Backscatter. A retroreflector is a device or surface that, unlike mirrors, *reflects light back to its source along almost exactly the same incoming direction with little scattering [8].* A retroreflector can be produced using spherical lenses or a corner reflector with three mutually perpendicular reflective surfaces. A large yet relatively thin retroreflector is possible by combining many small corner reflectors, using the standard triangular tiling. Cheap retroreflector material are readily available, *e.g.* the 3M Scotchlite Reflective Material Fabrics [1], and are widely used on road signs, bicycles, and clothing for road safety, especially at night.

The ability to bounce back light from any incidence angle to its source leads to a favorable *energy concentration* property of the retroreflector, as is illustrated in Fig. 2: light energy from a point light source being shed onto the surface area of a retroflector will be reflected back and concentrated to nearby the point light source.

2.2.2 Modulation with LCD Shutter. While retroreflectors can be used to modulate information bits, *e.g.*, by electronically controlling the reflection or absorption state using micro-electromechanical systems (MEMS) [12, 19, 33, 52] or semiconductor multiple quantum wells (MQW) technologies [21, 38], we hope to use off-the-shelf retroreflector fabrics for its thinness, flexibility and low cost. To modulate the lights reflected by such fabric, an LCD shutter that can pass or block light under the control of electrical field is adopted.

An LCD has a multi-layer sandwich structure. At the two ends of the LCD panel are two polarizer films whose polarization direction is fixed (often perpendicular to each other). In the middle are two glass electrodes that encompass a layer of nematic phase liquid crystal. Depending on the actual twisted or untwisted state of liquid crystal molecules, the polarity of passing light may be altered (called optical rotation [17]) or keep untouched, which will further cause

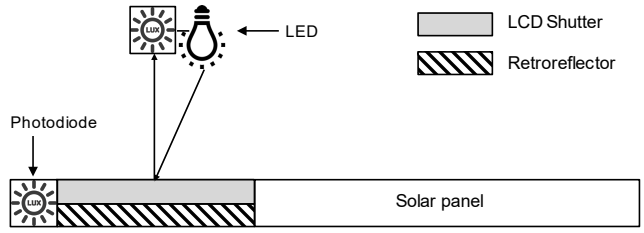

Figure 3: RetroVLC/PassiveVLC design illustration.

the light to pass or be blocked by the polarizer film. We thus can toggle the pass/block state of the whole LCD by imposing an electric field (through the two surrounding glass electrodes) on the liquid crystal layer. Note the liquid crystal molecules cannot instantly toggle between twisted and untwisted state. It typically takes in the range of few milliseconds, or termed as "response time", which fundamentally limits the data rate of OOK-based system [28].

3 SYSTEM DESIGN

The design of PassiveVLC overlaps with RetroVLC in its system architecture (§3.1) and circuit implementation (§3.2), but optimizes the software (de)modulation part of the retroreflecting link in terms of improving data rate (§4). In this section, we stay in the high level to recap the key components of RetroVLC/PassiveVLC.

3.1 Overview

The basic design of PassiveVLC is to backscatter the incoming light using a retroreflective fabric and to modulate it with an LCD shutter, as shown in Fig. 3. The overall system consists of a reader (ViReader) residing in the lighting infrastructure and tags (ViTags) integrated in mobile/IoT devices. A ViTag contains a light sensor, a retroreflective fabric, a transparent LCD shutter, solar panels and the control circuits, while a ViReader is a typical VLC device similar to [25, 29, 30, 43]. At a high level as shown in Fig. 4, PassiveVLC works as follows. For the downlink, the LED in ViReader switches on and off at a high frequency (*e.g.* 1 MHz, to avoid a human perceptible flickering), turning the illuminating light into a communication carrier. Information bits are carried using a certain modulation method and the light signals are picked up by the light sensor on ViTag and decoded therein. For the uplink, the same carrier is leveraged via reflection. The ViTag uses retroreflector to retrospectively reflect the light from lighting source and further carry information bits by remodulating this retroreflecting link – a solar-powered MCU electronically controls the state (pass/block) of the LCD shutter atop to realize OOK-trend based retrocommunication. The modulated reflected light carrier is then picked up by a photodiode on the ViReader and further demodulated and decoded.

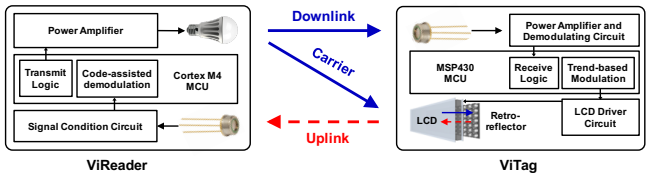

Figure 4: PassiveVLC system block diagram.

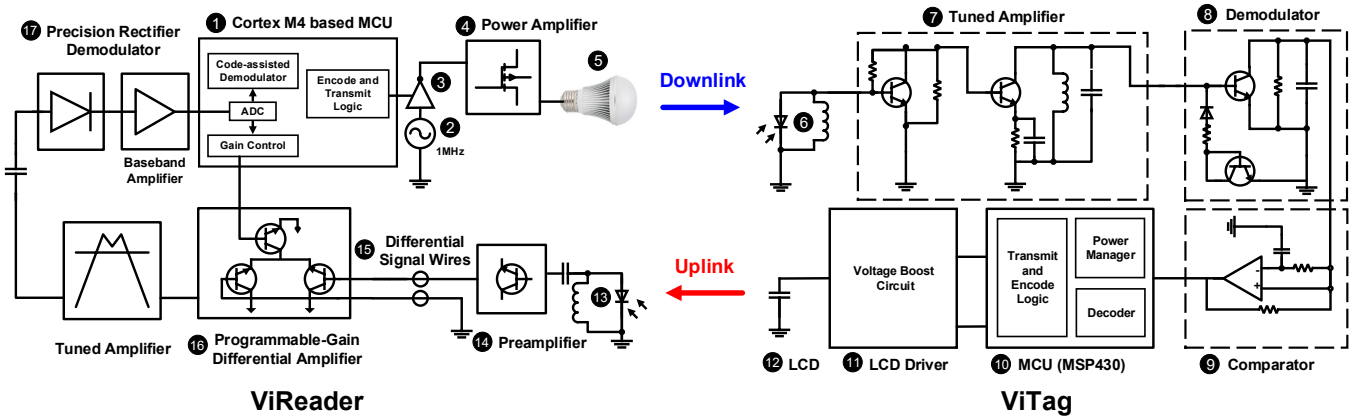

Figure 5: PassiveVLC circuit diagram: For ViReader-Tx, the information bits are first encoded by MCU ❶ into (clock period) coded signal while the carrier is generated by the oscillator ❷. The signal is then modulated by an amplifier ❸ and handed over to the power amplifier ❹ to drive the LED ❺ for transmitting the signal using visible light as the medium. For ViTag-Rx, the incoming light is first captured by the photodiode ❻ and turned in to electrical signal, which is then amplified and filtered by the tuned amplifier (for bandpass filtering) ❼. The demodulator ❽ extracts the baseband signal from the carrier. Then the signal is digitalized by a comparator ❾ before it is fed into the MCU ❿. For ViTag-Tx, the MCU ❿ performs (Miller) encoding and controls the LCD driver ⓫ to toggle the LCD ⓬ for modulating the reflected light. On the ViReader-Rx, the photodiode ⓭ captures the signal from the retroreflecting link, and the photocurrent is then amplified by preamplifier ⓮ to prepare for later transmission on wires ⓯. After that the signal is fed to the internal differential amplifier ⓰ through a pair of wires, such design suppresses the noises incurred by the long wires. The resulting signal is further demodulated ⓱ from the carrier and amplified before being into the ADC of MCU for code-assisted demodulation and decoding ❶.

3.2 Circuit Design

The circuit design of PassiveVLC is similar to RetroVLC [28] except for a minor change: we replaced the RC oscillator with a crystal oscillator. This change incurs a small energy consumption overhead on MCU from 23 μW to 26 μW, but significantly reduces system's clock drift, and thus improves link reliability, especially under temperature changes. Fig. 5 provides a detailed description of the overall operational flow of PassiveVLC and the functionality of each module in circuit level.

4 RETROREFLECTING LINK DESIGN

The key to PassiveVLC's design is the retroreflecting link. While the current circuit design addresses the challenges rooted from detecting the extremely weak and noisy reflected signal as well as the low power (sub- mW) requirement [28], one of the key contribution in this paper is the trend-based modulation and code-assisted demodulation design for optimizing the link speed of the retroreflecting link. In the rest of this section, we will elaborate the design of our modulation and coding schemes as well as their interaction.

4.1 Trend-based Modulation

The nonlinearity nature of the LCD shutter makes OOK the most feasible solution when it is used as the modulator [41]. In other words, LCD is turned on/off completely when in use [28, 41]. The potential inefficiency of this solution is that we will have to wait until the LCD completely change its on/off state before modulating the next symbol. Therefore the minimum interval for modulation or modulation bandwidth is highly limited by the response time of the LCD T_r – time needed for the LCD to switch between on and off

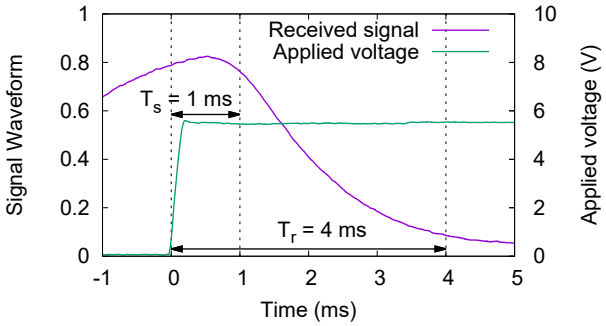

Figure 6: LCD signal in response to applied voltage.

states when we change the voltage applied to it. According to the measurements in our ViTag, it takes about $T_r = 4\ ms$ to completely change the state in response to the voltage change.

To boost bandwidth, we observe that as soon as the LCD is charged or discharged, even if incompletely, the level of its transparency will change over short time. The resulting *trend* of the voltage change on the receiver side already conveys the information. As shown in Fig. 6, a $T_s = 1\ ms$ period after voltage change is long enough to produce a distinguishable decreasing trend on the receiver side, which means that 1 ms can be used as a minimum modulation interval to deliver 1 $kbps$ data rate theoretically and 4x larger bandwidth in our case.

Specifically, while modulating a symbol '0', we discharge the LCD to increase its transparency level, resulting in an increase trend in the received waveform at ViReader-Rx. Similarly while modulating

a symbol '1', we charge the LCD to decrease its transparency level, which leads to a decrease trend in the received waveform.

However, such trend-based modulation scheme has its weakness – it does not allow long consecutive '0' or '1' sequence since such sequence will generate a DC component in the received signal after the LCD is turned on or off completely, which is hard to catch by conventional amplifiers and vulnerable to ambient light shifts. Therefore, the design or choice of the coding scheme is critical in solving this issue.

4.2 Coding

As discussed earlier (§4.1), the coding design needs to accommodate the situation when a long stream of ones or zeros are to be sent. In RetroVLC [28], the use of Manchester coding solve this issue because it ensures that no more than 2 consecutive symbols of same type appear in the encoded symbol sequence. However, it consume up to approximately twice the bandwidth of the original signal under the same minimum modulation interval. Therefore, we utilize Miller encoding, which maintains the property of accommodating long stream of ones or zeros, but without compromising the data rate. As shown in Fig. 7: A bit '0' is modulated to two identical symbols. These symbols are of the same type to the previous symbol if the previous bit is '1', otherwise a different type is used for these two symbols. A bit '1' is modulated to two different symbols. The first one is of the same type to the previous symbol.

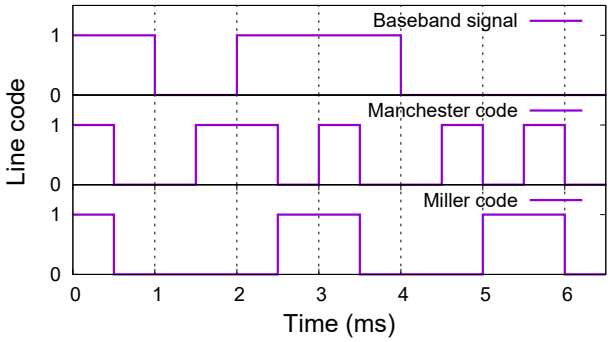

Figure 7: Example of Manchester coding and Miller coding.

Miller encoding has a property that only 2, 3 or 4 consecutive symbols of same type will appear in the encoded symbol sequence, which, on the one hand solves the problem of consecutive same-type symbols, and on the other hand, requires no smaller modulation interval compared to directly sending the information bits (though double the symbol rate).

To make the property mentioned above still holds for the very first symbol, a meaningless symbol '0' is padded before the symbol sequence, and the first symbol of the first bit is set to '0'. Besides, a special waveform is transmitted before the symbol sequence as preamble, helping to determine the precise timing of the symbol sequence as well as the signal strength.

The decoder for Miller encoding is simple as follows. We first drop the very first padding symbol. In the rest, every 2 symbols represent a bit – two identical symbols produce a '0' in the bit sequence, while two different symbols produce an '1'.

4.3 Code-assisted Demodulation

Demodulation is the process to recover the symbol sequence from the received and sampled waveform. In most cases, demodulation is straightforward as each symbol can be demodulated independently. However, in our case, we use a specially designed modulation scheme, which makes demodulation more complicated:

- Symbols are not independent with each other. The waveform of a symbol is affected by the previous ones.
- The waveform of a symbol is also related to the state of the LCD. For example, modulating an symbol '1' to an LCD in the fully off state will not cause the voltage on the receiver side to drop any more.
- Due to the coding scheme, not all possible symbol sequence is valid. We should take advantage of this property, producing only valid symbol sequence as output of the demodulation algorithm.

Conventional demodulation methods demodulate each symbol independently and thus fail to cooperate with trend-based modulation we use here, especially at high data rate when the trend is short and it is relatively challenging for symbol recognition. In contrast, by embracing these properties above, we aim to develop a novel demodulation design for our system to boost the link speed.

4.3.1 Demodulation at Sequence-Level. The straightforward way to independently demodulate each symbol has weaknesses:

- *It can't take advantage of the dependency between symbols.* As an example, the 5th symbol in Fig. 8 is more likely to be '0' when treated independently. But it's actually an '1' which can be easily identified when we take the previous and the next symbol into consideration.
- *It can't guarantee a valid output sequence.* As an example, the fact that at most 4 consecutive symbol '0' can occur in a valid symbol sequence could have saved us from regarding the 5th symbol in Fig. 8 as '0'. By demodulating each symbol independently, we lost the last chance to do so.

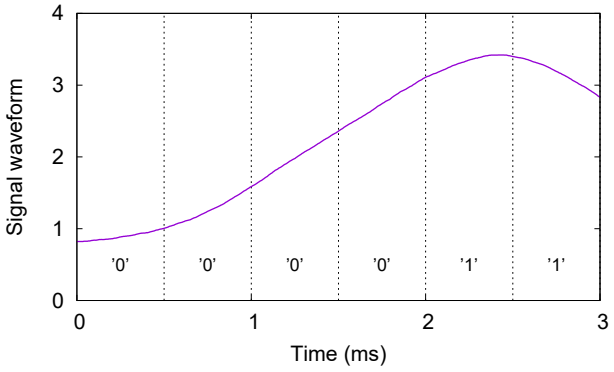

Figure 8: Waveform that fails conventional methods.

In order to overcome these weaknesses, we need to demodulate at sequence level instead of individual symbols. Inspired by Dynamic Time Warping (DTW) [10], we can formulate the demodulation problem as an optimization problem for multistage decision processes rather than several independent decision problems, to take

symbol dependencies into consideration as well as the restrictions exerted by sequence validity.

Here, we demodulate by "optimally" (§4.3.2) decomposing the received waveform into segments where each segment represents consecutive symbols of same type. According to the properties mentioned in §4.2, some restrictions apply: Each segment should consists of 2, 3 or 4 symbols; Segment of 4 symbols can only occur after even number of symbols in the symbol sequence. In addition, minor error in timing should be to tolerated in case of possible clock skew and clock drift. That is, we should allow segments to overlap or separate a little bit in our decomposition.

4.3.2 Optimality of Decomposition. In §4.3.1 we formulate the demodulation problem as an optimization problem. But the definition of optimality remains unclear. To define optimality, a quantitative index for how likely that a decomposition is correct for a certain waveform is critical. Therefore we proposed *Match Score*.

The *Match Score* for a certain decomposition is defined as the sum of all its segments' *Match Score*. The *Match Score* of a segment is defined as the similarity of its waveform to the corresponding reference waveform.

But how to quantify the similarity of two given waveforms $\mathbf{X}$ and $\mathbf{Y}$, both of the length n? In some existing systems like CDMA, correlation coefficient $\mathrm{corr}(\mathbf{X}, \mathbf{Y})$ is used. But this is not suitable for us since we need to sum up the *Match Score* of segments, while the sum of correlation coefficients is meaningless, especially when segments are of different length. Therefore, we decide to develop a new 'addable' index.

An intuitive idea is to use the following formula:

$$NaiveSim(\mathbf{X}, \mathbf{Y}) = \sum_{i=1}^{n} (\mathbf{X}[i] - \mathbf{Y}[i])^2$$

However, this formula is not practical because: It does not take into account the fact that the amplitude and mean of the waveform may vary from symbol to symbol. Therefore, the following formula, in which a scale factor a and an offset b are applied to adaptively adjust the amplitude and mean of the waveform, is used to address this problem. In other words, we normalize the two waveforms in a way that minimize the *Match Score*.

$$\begin{aligned} Sim(\mathbf{X}, \mathbf{Y}) &= \min_{a \geq a_{\min}, b} NaiveSim(a\mathbf{X} + b, \mathbf{Y}) \\ &= \min_{a \geq a_{\min}, b} \sum_{i=1}^{n} (a\mathbf{X}[i] + b - \mathbf{Y}[i])^2 \end{aligned}$$

where $a_{\min}$ denotes the minimum scale allowed to prevent the waveform from degrading or flipping, which is a positive number usually set proportionally to the scale we obtained from preamble. As we calculate, the minimum value of the formula can be obtained when

$$\begin{aligned} a &= \max\left(\frac{n\sum \mathbf{X}[i]\mathbf{Y}[i] - \sum \mathbf{X}[i] \sum \mathbf{Y}[i]}{n\sum \mathbf{X}[i]^2 - (\sum \mathbf{X}[i])^2}, a_{\min}\right) \\ b &= \frac{1}{n}\left(\sum \mathbf{Y}[i] - \sum a\mathbf{X}[i]\right) \end{aligned}$$

Fig. 9 gives an example of how it works, where $\mathbf{X}$ denotes a possible waveform of consecutive symbol '1', $\mathbf{Y}$ denotes the corresponding reference waveform, $a\mathbf{X} + b$ denotes the normalized waveform of $\mathbf{X}$. In this case, $a = 3.4240, b = -4.2567, Sim(\mathbf{X}, \mathbf{Y}) = 1.0786$.

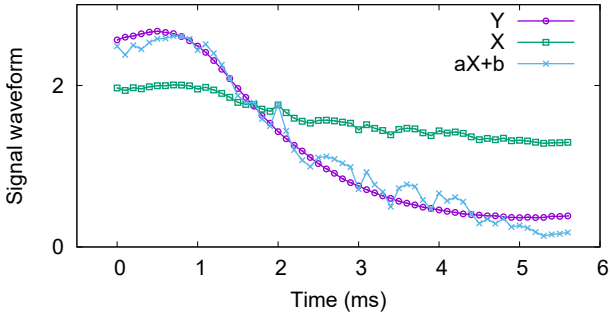

Figure 9: An example illustrating the effect of a and b.

Now we can formally define the *Match Score* of a segment as the *Sim* value of its waveform and the corresponding reference waveform. More specifically, let l_{sym} be the waveform length of a single symbol, n_{seg} be the number of symbols in the segment, $\mathbf{W}$ be the waveform of the segment, $\mathbf{R}(t, n_{\mathrm{seg}})$ be the reference waveform of n_{seg} consecutive symbol of type t ($t = 0, 1$) , then the *Match Score* of the segment being n_{seg} consecutive symbols of type t is defined as:

$$MatchScore(\mathbf{W}, t, n_{\mathrm{seg}}) = Sim(\mathbf{W}, \mathbf{R}(t, n_{\mathrm{seg}}))$$

Note that the LCD may reach a fully on/off state, producing a level part (approximately) in the end of the waveform. These level parts should not be taken account in the calculation of *Match Score*.

4.3.3 Problem Formalization. Now let's formally define the optimization problem for demodulation. Let $\mathbf{S}$ be the received waveform, n be the number of symbols to demodulate, l_{sym} be the waveform length of a single symbol, err be the maximum timing error allowed in samples (which is usually set proportionally to l_{sym}), $Start$ be the position where the symbol sequence start (which can be obtained by searching preamble), the optimization problem can be formulated as:

$$\begin{aligned} \min_{p_i, s_i, m} \quad & \sum_{i=0}^{m-1} MatchScore(\mathbf{S}[p_i \ldots p_i + s_i l_{\mathrm{sym}} - 1], i \bmod 2, s_i) \\ \text{s. t.} \quad & -err \leq p_0 - Start \leq err \\ & -err \leq p_i - p_{i-1} + s_{i-1} l_{\mathrm{sym}} \leq err \quad (1 \leq i < m) \\ & 2 \leq s_i \leq 3 \quad \left(\textstyle\sum_{j<i} s_i \text{ is even}\right) \\ & 2 \leq s_i \leq 4 \quad \left(\textstyle\sum_{j<i} s_i \text{ is odd}\right) \\ & n = \sum_{i=0}^{m-1} s_i \end{aligned}$$

where m denotes the number of segments, s_i denotes the number of symbols in the ith segment, p_i denotes the very first sample of the ith segment.

(a) Indoor office: 200 lx (b) Outdoor cloudy day: 2000 lx (c) Outdoor night: 10 lx

Figure 10: Evaluation testbed setup with a pair of ViReader and ViTag.

4.3.4 Solving the Optimization Problem. So far we formulate the demodulation problem to an optimization problem for multistage decision processes. This problem can be solved using Dynamic Programming. The symbol sequence can be constructed through the process of dynamic programming.

While implementing the dynamic programming algorithm, an optimization is used to speed up the calculation: Instead of running the algorithm after all symbols are sampled, we solve a subproblem as soon as the required sample values for that subproblem are sampled. As measured in §5.3.2, the time required to solve all the subproblems related to a symbol is less than the time of a symbol, resulting in an almost real-time demodulation.

5 EVALUATION

In this section, we present the experimental results from our prototyped PassiveVLC– a 3 W modified flashlight as ViReader and a battery-free ViTag. Here are the highlighted results:

- **Link performance:** ViTag operates at up to 1 $kbps$ on a loss-free uplink when it is within 1 m from ViReader. PassiveVLC works for a flexible range of ViTag orientations up to ±60° and under different ambient light condition (from dark chamber, outdoor night, indoor office to day light).
- **Energy Consumption:** PassiveVLC adapts to different data rate (0.25, 0.5 and 1 $kbps$) under a 150 μW power budget and achieves sub-μJ per bit.

5.1 Prototype Implementation

We implemented PassiveVLC system shown in Fig. 1. The ViTag is battery-free – it harvests light energy from the on-board solar panel. The size of ViTag is 8.2×5.2 cm, same as a credit card. About two-thirds area is used for solar cells and the rest for the LCD and retroreflector. The ViReader is modified from a flashlight which uses a 3 W white LED as the transmitter. Three photodetectors are used in serial to improve the SNR. The overall cost of each ViTag is about $8 and even less when in mass production.

5.2 Experimental Setup

We evaluate PassiveVLC using our prototype implementation with a testbed shown in Fig. 16. We carried most of the experiments in typical office environments, where the ambient light is maintained in a comfortable range around 200 lx. As ViReader is externally powered and the downlink signals are strong[1], we have thus focused on measuring the *bottleneck uplink performance*. We mount our system on a robot and programmably control the movement of our ViTag or ViReader to the desired position and orientation. The system parameters include distance (between ViTag and ViReader), incidence angle (ViTag), irradiation angle (ViReader), data rate (uplink), packet length (uplink) and FoV (reader). The default setting is summarized in Tab. 1. For each parameter setting, the ViTag continuously sends 100 packets (4-$byte$ ID data for each) to ViReader with a constant rate and we take the average to report our results.

5.3 Micro-benchmarks

5.3.1 How reliable is the retroreflecting link? We use the packet loss rate (PLR) as the primary metric to answer this question. For VLC, the received signal strength is mainly affected by two factors,*i.e.* the distance between ViTag and ViReader and the incidence angle [29]. In addition, we would also like to see whether the packet length or ambient light condition will affect the link reliability.

Distance. We first measure the impact of distance on PLR by varying the Line-of-Sight (LoS) distance between ViReader and ViTag. We count the number of packets correctly received at ViReader under different data rate. From Fig. 11(a), we make two observations: First, when ViTag is sending bits faster, it also has a higher PLR. This is because when the LCD is not fully "open" or "close", the resulting low on/off ratio effect will decrease the signal strength. Second, under a fixed bit rate, ViTag maintains a fairly stable loss-free uplink until reaching a certain distance. This is because a lowest SNR, which is often called as sensitivity, is needed for ViReader-Rx to

[1]We used a 2.5 $kbps$ downlink in our experiments.

Parameter	Value	Note
Distance	1 m	Line-of-Sight
Incidence angle	0°	See Fig. 3 for illustration
Irradiation angle	0°	See Fig. 3 for illustration
Data rate	0.25 $kbps$	Baseline value in our test
Packet length	32 bits	Typical value for RFID tag
ViReader's FoV	4°	Default manufacture setting

Table 1: Default parameter setting for experiments.

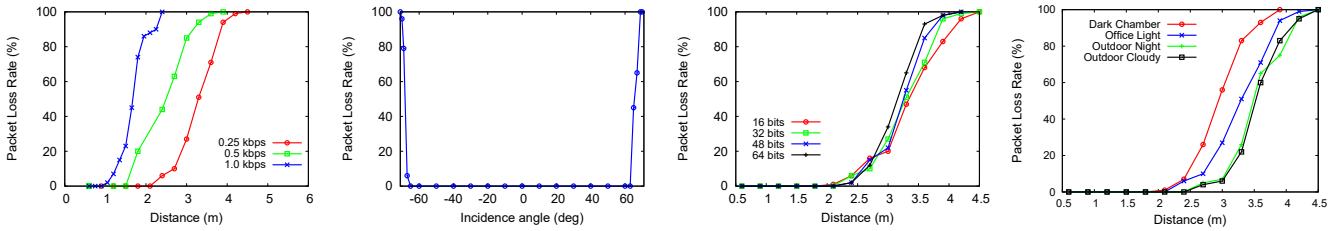

(a) Uplink bit rate (b) Orientation of ViTag (c) Packet payload length (d) Ambient light condition

Figure 11: The performance of packet loss rate (PLR).

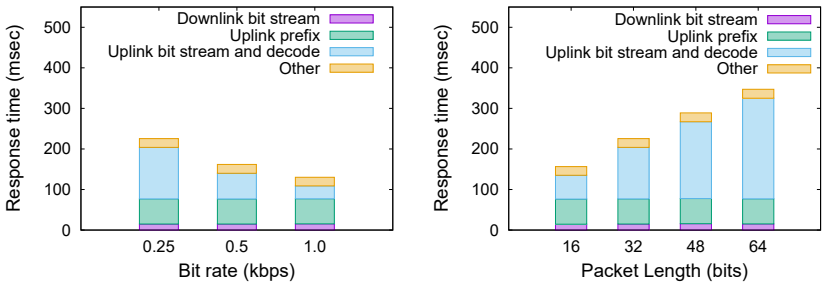

(a) Bite rate (b) Packet length

Figure 12: The performance of response time.

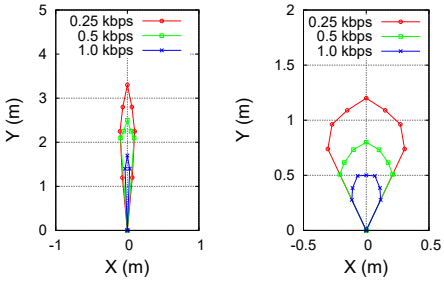

(a) Focus FoV (b) Wide FoV

Figure 13: Working range.

demodulate the backscattered signal. And with longer distance, the backscattered signal will suffer from a higher channel loss, which will be discussed further in §6.

Incidence Angle. We then evaluate the PLR under different incidence angles corresponding to the orientation of ViTag. In this experiment, we fixed the distance between ViReader and the ViTag at 1 *m*, and varied the orientation of the ViTag. The purpose of this experiment is to evaluate how flexible ViTag's orientation can be while maintaining a reliable link. Fig. 11(b) shows that when ViTag maintains a loss-free uplink when its incidence angle is between -60°and 60°. Thanks to the high coefficient of retroreflection on our retroreflector, it is able to concentrate the reflected light automatically and thus has a high gain in a wide range of orientations. Once the harvested energy is below the sensitivity level (± 65°or so in our case), the PLR drops to 100% in a sharp manner.

Packet Length. Packet length is another variable of interests regarding to PLR as it represents the needs of different IoT applications, such as identification, sensor data, *etc.*. In Fig. 11(c), we observe that a longer packet results in higher PLR in general. However, when ViTag is close to ViReader (< 2.7 *m*, typical distance between illuminating infrastructure and IoT devices in indoor environments), the PLR difference is marginal (< 5%). This is a desirable outcome because it illustrates that despite a long packet increases the bit error rate in theory, the length does not play a key role in increasing PLR when the link is relatively short, as in most cases.

Environmental Impact. So far in our experiments, the ambient lighting conditions are limited to office environments. In typical VLC systems, ambient light only plays a "negative" role – a strong lighting source can easily saturate the light sensor and make the receiver fail. Interestingly, there is such a trade-off in PassiveVLC system: on the one hand, the ambient light introduces the same challenge to the optical receiver side; on the other hand, a higher energy harvesting efficiency can potentially reduce the ViTag size or increase the communication range. We measure the PLR under different ambient light conditions. As shown in Fig. 11(d), we obtain the best results (in terms of the lowest PLR under same distance) in outdoor daytime and the worst in a dark chamber, as expected. Interestingly, we observe that the results from outdoor night outperform the ones from office environments. This is because we often have more lighting infrastructure in the vicinity which can bring unexpected noise. Overall, we demonstrate that PassiveVLC performs almost equally well under a variety of ambient lighting conditions. Note that PassiveVLC can't work when either ViTag or ViReader is under direct sunlight. However, this is a general problem with VLC, not unique to our system.

5.3.2 Response Time. Response time is defined as the time from the ViReader issuing a query to receiving a response from the ViTag. Therefore, a series of components in the downlink and uplink (encoding, prefix, preamble, bit stream, decoding) account for the response time in order. We experimentally segment these modules, report the timing breakdown results in Fig. 12. Note that we only show part of the components which are highly relevant to the uplink design. The rest accounts for only 10% of the total response time. In Fig. 12, we observe that the time spent on uplink bit stream is linearly proportional to the bit rate and the packet length, which is expected. Note that our current design has a relatively long constant delay (63 *ms*) for uplink prefix. This is because the downlink transmission causes a huge impulse in the on-board power supply module and other signal lines. Within several stages of amplification, the impulse will cause saturation in the last stage amplifier, which means that the reader cannot process any signal during that

time. As a result, we add a fixed pattern of prefix before the uplink payload. The prefix also serves as the timing initialization in the decode process. We plan to improve our hardware design to reduce its impact in the future. Finally, we acknowledge that the current design of PassiveVLC is not very efficient in terms of response time – the ViReader can only issue at most 10 queries per second at the highest rate (1 *kbps*) we achieved. We have a dedicated discussion on that in §8.

5.3.3 Working Range. Another important question to ask is: how far the ViTag can be away from the ViReader while still maintain an acceptable data link. Here we define the working range as the area within which the ViTag can harvest enough energy and talk with the ViReader with a chance above 50%, *i.e.*, PLR is less than 50%, and measure the working range in office environments. Specifically, in this experiment we also adjust the FoV of the flashlight to its maximum (35°) therefore it is expected to work in a wider but shorter range. The working range in Fig. 13 is the area within the closed curve. First, we observe that a lower data rate link leads to a larger working distance in terms of both depth and breadth, and the reason is similar as discussed in §5.3.1. With an upright orientation of the ViTag, the maximum working distance is up to 3.3 *m*. Second, the angle of the working range is roughly equal to the FoV of the lighting source. This is to be expected and in fact is a favorable feature because based on it we can predict and control the "width" of the working range. We note that PassiveVLC's working range can be further extended with more energy harvested. A emulation-based analysis is provided in §6.

5.4 Energy Consumption

Measuring the energy consumption is always critical for understanding the design trade-off (data rate, form factor, *etc.* in our study) and finding optimization opportunities. In this experiment, we disconnect the solar panel from our tag and use Monsoon [5] to measure its power consumption. We power ViTag at 2 V because it's the minimum and safe operating voltage for the on-board MCU to work. We operate the PassiveVLC as usual and shows the time-series power consumption snapshot on the ViTag in Fig. 14. We can see that in each query, ViTag spends 23 *ms* in listening, which accounts for 678 μW and 15.6 μJ in total. This part of the energy is mostly spent on the static current of the analog circuit for signal detection. In other words, the receiving circuit is always on because ViTag never knows when it is expecting an incoming signal. We can address this deficiency with an efficient MAC protocol design. Then the ViTag receives the downlink bit stream and encodes the content to response, which consumes 373 μW. After that it turns off the receiving circuit and starts to transmit. In the transmission stage, ViTag spends less than 117 μW on average at the highest bit rate, which is much lower than mW-level LED-based transmission. We also see that ViTag spent more power in transmission but less energy per bit when it operates at a higher bit rate.

Overall, we demonstrate that with such a low energy budget, we are able to drive it by harvesting light energy using only small solar cells (a more detailed analysis is provided in §5.5). We summarize the break-down power/energy consumption for each query in Tab. 2.

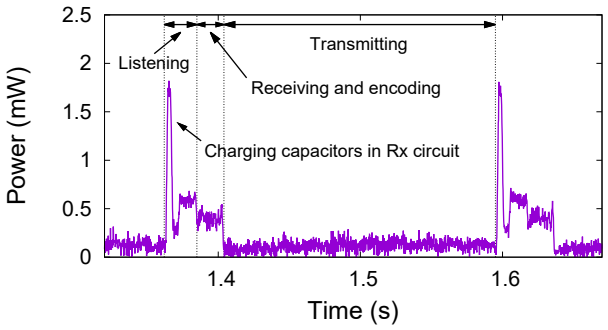

Figure 14: Snapshot of power consumption on ViTag.

Component \ Bit rate	0.25 *kbps*	0.5 *kbps*	1.0 *kbps*
Backscattering state	95 μW	108 μW	117 μW
Receiving state	373 μW	398 μW	408 μW
Average power	97 μW	113 μW	152 μW
Energy per bit	0.38 μJ	0.22 μJ	0.12 μJ

Table 2: Energy consumption of ViTag per query.

5.5 Size Tradeoff

In our ViTag implementation, we dedicate two-thirds of the area to solar cell and one-third to retroreflector. It is natural to ask: is this ratio the right choice or even the golden rule?

From Tab. 2, we observe that in the process of a query, peak power happens in the receiving state. In addition, the passive nature of PassiveVLC determines that the receiving phase is ahead of the backscattering phase, which results in a more challenging requirement for energy harvesting. For instance, in the case of 0.25 *kbps*, the power provided by solar panel needs to meet the requirement of the peak power (373 μW) instead of the (much lower) average power (97 μW).

Our measurements show that in the dark chamber, the LED flashlight casts 240 *lux* at the solar panel from a distance of 5 *m* away. In turn, one single solar cell (at the size of 54×27 *mm*) is able to provide 196 μW at 1.98 V. Therefore, the two cells we use are able to provide 392 μW to cover the required energy consumption. Note that this energy harvesting measurement is conservative – the ambient light intensity is often larger than 200 *lux* and thus more energy can be harvested for powering ViTag. To this end, our experimental measurements justify the ratio in our prototype.

Furthermore, the aforementioned scenario assumes a continuous communication is required. If the communication process can be intermittent, then the power requirements can be relaxed because in practice it just takes the solar panel more time to harvest the energy to reach the operating voltage.

6 LINK BUDGET ANALYSIS

Much like the link budget analysis on RF links [7], it is desirable to perform similar analysis for PassiveVLC to understand the relationship and trade-off among the involved key factors such as device's form-factor size, transmitted power of the illuminating infrastructure and the communication distance. For instance, when

Symbol	Parameter
P_t	Transmission power of the light source
G_t	Directional gain of the light source
G_{re}	Directional gain of the retroreflector
L_m	Loss through LCD modulator
A_{re}	Projected area of retroreflector
A_r	Projected area of photodiode in ViReader-Rx
R	Communication distance
θ	Irradiation angle, see Fig. 15 for illustration
α	Observation angle, see Fig. 15 for illustration
β	Incidence angle, see Fig. 15 for illustration

Table 3: Parameters in link budget analysis.

our ViReader is integrated into car's headlight for the purpose of recognizing road sign or pedestrian at least 30 m away, what's the required minimum size of ViTag? As another example, when a ViReader-enabled ceiling light wants to talk to the IoT devices placed in indoor environments, what is the suggested transmission power of the lighting infrastructure? Intuitively, a small increase in range will lead to a significant increase in path loss. To compensate for that, one simple solution is to adopt a larger retroreflector-LCD suite to concentrate more energy for the uplink budget. However, a larger LCD comes with more energy consumption, and in turn needs a larger solar panel. Hence, a systematic analysis would provide insights for guiding real application deployment.

For a retroreflector-based visible light backscatter communication system with LCD modulators, we propose a model (with all the parameter definition in Tab. 3) to count in the transmission power of the light source and all the factors of the gains and losses from the transmitter and the visible channel medium (downlink, retroreflector, LCD, *etc.*). The energy received by the photodiodes of ViReader is as follows:

$$P_r = P_t G_t \frac{A_{re}}{4\pi R^2} G_{re} L_m \frac{A_r}{4\pi R^2}$$

In this equation, there are six factors contributing to the two critical phases which we will elaborate in the rest of this section.

6.1 Power budget of Passive/Retro Transmitter

The transmission power of the uplink actually originates from ViReader-Tx. The radiated on-path light energy is determined by P_t and $G_t(\theta)$ (transmission power and directional characteristics of the light source) often modeled by Lambertian model [9]. In other words, these two factors together indicate how strong the downlink light beam is emitted towards the ViTag.

The third factor characterizes the downlink path loss and how much energy can be collected by the retroreflector of area A_{re} at a distance of R from ViReader-Tx, which is similar to Friis free space equation in radio propagation. In our case, thanks to its energy concentration property (Fig. 2), a larger retroreflector can harvest more energy for backscattering and thus improve the SNR of the received signal and potentially increase the communication distance. However, we note that it is not always practical to reply on increasing the retroreflector's area to extend the distance. The linearity can be easily overwhelmed by the square factor in power attenuation, let alone the attenuation factor becomes quadratic when considering the uplink together.

6.2 Path Loss of Retrocommunication

The first three factors compute the amount of energy captured by ViTag. The next step is to determine how much the backscattered energy can reach at the photodiodes or light sensor in ViReader-Rx.

Typical omni-directional antenna has relatively low directional gain because the energy disperses in all directions. However, thanks to the auto-focus feature of retroreflectors, it is possible to meet both high gain and wide angular range at the same time. G_{re}, the directional gain of the retroreflector, plays a key role here. To be more specific, G_{re} is equal to $R_A(\alpha, \beta)$, the retroreflection coefficient of the material, which determines how much energy it can concentrate for retroreflection given the incident light beam at a certain incidence angle β, to a certain observation angle (towards to the light sensor) α, deviated from the incident light. [2] While α is determined by the communication distance once the relative position of led and photodiode is fixed, β is directly associated with how flexible the orientation of ViTag can be when point to ViReader. For visible light backscatter systems, it is desired to have such material with a high R_A and it is insensitive to β at the same time. For the commodity retroreflectors [1] we use, it has an R_A of 500 $cd \cdot lx^{-1} \cdot m^{-2}$ ($\beta = 5°, \alpha = 0.2°$), which leads to a G_{re} of 27 dBi. In addition, R_A only attenuates 5 dB as β reaches to 40 °. Our evaluation shows that at $\beta = 60°$, the gain is still sufficient to support an uplink transmission in 1 m. On the other hand, when β is fixed, R_A stays high only within a small α (typically less than 1 °) and attenuates sharply as α rises above 1.5 °. In Fig. 15, we show the illustration of the energy distribution of the reflected in gray scale. The resulting concentrated and narrow reflected beam suggested the placement of the light sensor is crucial in improving the SNR of the uplink.

L_m, the energy loss when light passes through the LCD modulator, also impacts the backscattered signal strength. In our system, the incidence light will pass through the LCD twice, before and after the retroreflection. Due to the polarizing nature of the LCD [2], a beam of non-polarized light becomes polarized after passing through and lost 50% power. Coupled with other factors (such

[2] An illustration of these angles can be found in Fig. 15.

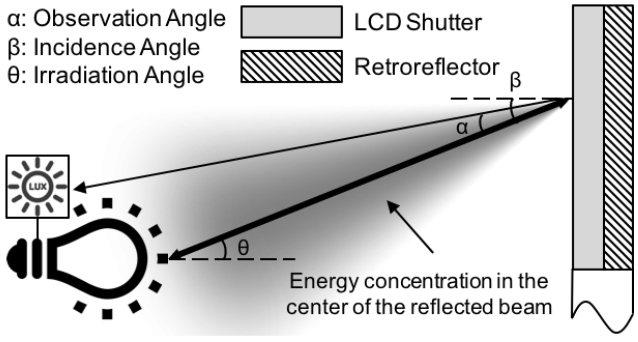

Figure 15: Reflected energy concentrates in a narrow observation angle of about 1.5 °.

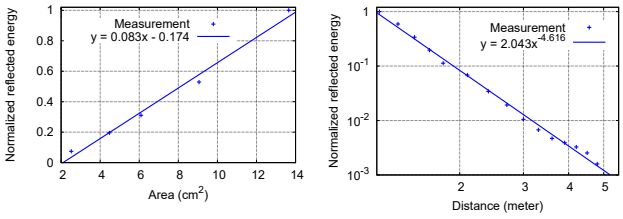

(a) Area of retroreflector (b) Communication distance

Figure 16: Model fitting for link budget analysis.

as absorption of liquid crystal), our measurements show that the power loss for the first time passing through the LCD is approximately 65%. The case of the second time is much more complicated because the retroreflector may change the polarization direction of the light, and it is challenging to measure the loss because the incident and outgoing light beams overlap in space. We estimate this loss as 50%[3] and thus L_m is approximately -7.6 dB. In addition, L_m also is also relevant to the data rate because when the LCD (dis)charging time is reduced, the amplitude of the modulated signal is "attenuated"as well. In our measurements, compared with the case of 0.25 $kbps$, the extra loss at a rate of 0.5 $kbps$ and 1.0 $kbps$ is 7.7 dB and 20.4 dB respectively. Note that this measurement is based on our ViReader-Rx module, and thus it includes the impact of the variant frequency response in our circuit implementation when ViTag operates at different data rate.

We have conducted several controlled experiments to verify our analysis. First, we change the area of retroreflector A_{re} and fix other parameters. The results shown in Fig. 16(a) demonstrate that received signal strength (square of the ADC voltage reading) is linearly proportional to A_{re} with R^2 of 0.9886. Next, we fix A_{re} and change the communication distance R and plot the results in Fig. 16(b). We make a linear fit of the received signal strength and the distance in log scale. The results show that the received signal strength is inversely proportional to 4.6th power of the distance, which fits our model well with R^2 of 0.9953. Note that our measurement starts at 1.2 m because the ADC is saturated from a closer location. However, PassiveVLC can still work at the distance of [0.6,1.2] m as long as we operate the average voltage when trend-based modulation is applied away from the saturation region.

7 PROOF-OF-CONCEPT APPLICATIONS

We evaluate two proof-of-concept applications to show how PassiveVLC applies to real world scenarios.

7.1 Smart Check-in System

Most existing smart check-in systems use RFID card, fingerprint or iris based identification techniques which requires a user in proximity. We argue that when bearing with ViTag a badge, PassiveVLC users can potentially enjoy a seamless experience when passing by different check-in points – a ViReader-enabled door will automatically grant the access when a authenticated PassiveVLC user is heading up into its working range, *e.g.*, from 2 m away. Thanks to the directionality of light, PassiveVLC can mitigate the false positives in RFID's case.

To evaluate the usability of PassiveVLC system in such scenario, we mount our ViReader prototype on the ceiling at 2 m in front of a door with a dip angle of 40 ° to ensure a 0.5 m of working range on the floor derived from the analysis of ground projection of the light cone. The number of 0.5 m is chosen to account for both PassiveVLC's response time (225 ms) and human walking speed (1 m/s). We ask five male and female subjects to wear our ViTag badge at different height (1, 1.05, 1.1, 1.15, 1.2 m) and head up towards the door at their natural walking speed. We count a test "successful" as ViReader is able to receive the ViTag's response without issuing retries. We conduct 100 tests in total and our experimental results show PassiveVLC achieve 90% of success rate.

7.2 Optical IoT/Sensor Networking

The second use case we present is optical IoT/sensor networking. Home/office sensors (motion, temperature, humidity *et al.*) can be integrated into ViTag and their sensory readings can be streamed to a ViReader-capable lighting LED infrastructure. PassiveVLC brings two benefits in this scenario: Firstly, it reduces the deployment cost because of its battery-free property. Secondly, it avoids the interference with other existing RF-based devices.

We instrument a wide FoV ceiling lamp of with our ViReader and place 1 to 5 ViTags in different locations (table, chair, TV, *etc.*) but still within ViReader's view. Each ViTag is assigned a unique ID and will response to ViReader's ID-based interrogation with 4-byte sensor data. The time to finish polling all the present ViTags are 0.225, 0.45, 0.675, 0.9 and 1.125 sec when 1 to 5 ViTags deployed respectively. We observe this "perfect" linearity because PassiveVLC is not running any operating system and thus all the operations can be scheduled into cycles precisely. We note that a complete PassiveVLC polling system requires a scanning/initialization phase as well as a MAC protocol, which we leave for future work.

8 DISCUSSION

Non-Line-of-Sight (NLoS). Due to the directional propagation property of light, PassiveVLC gains certain intrinsic security benefit such as sniff-proof, but it also suffers from an intrinsic limitation - it cannot work in NLoS situations, as any VLC system does.

Data Rate. The data rate or response time of PassiveVLC is doomed by the LCD shutter's turn-over rate, which may further limit its application to those low data rate IoT applications. There are several handy ways to improve the data rate to some extent. For example, instead of using a black-white LCD, color LCDs can be used to enable more communication channels. Accordingly, color filters should be added on the receiver side to distinguish different channels. As another example, one can use a plural of retroflectors and LCD shutters to achieve almost linearly increasing data rate, as evidenced in [41]. We further believe, once the technology is widely adopted, the market demand will stimulate the production of faster LCD shutters. Finally, devices other than LCD, e.g., digital micromirror device (DMD) can be treated as a promising modulator candidate – it can achieve tens of $kbps$ with 100 mW power budget

[3]When the linearly polarized light is reflected by the retroreflector, the orientation of the polarized light is evenly distributed in all directions. Therefore the polarizer will decrease the reflected light intensity by about 50%.

[3], and it can be useful for IoT device with a larger surface, such as road sign, cloth fabrics *etc.*

Networked Operation. We have primarily focused on the communication aspects of a single ViTag-ViReader pair. When many of these devices (both ViTag and ViReader) are in range of each other, we need mechanisms to arbitrate the channel access. We have designed a simple query-response MAC similar to that of RFID and applied in the second proof-of-concept application. Unlike RFID which is completely passive, the solar panel can continuously harvest light energy from ambient light, it may initiate a communication session to the reader. Thus, the MAC needs to be slightly modified to accommodate this new situation. We have omitted this part for sake of space constraint.

9 RELATED WORK

PassiveVLC is inspired by the idea of (radio) backscatter communication but differ from that by using visible light as the medium to achieve low power communication.

Visible Light Communication Systems. There have been many efforts exploring communication mediums wherein visible lights carry information. Most works, however, either deal with only one-way communication without an uplink [14, 24, 26, 45], or go in a two-way fashion with both sides supplied by battery [13, 16, 27], which limit the practicality for real-world deployment. Specifically, LED-to-phone systems [25, 29, 39] only support downlink transmissions, targeted at phone localization. LED-to-LED systems [40, 47] consider visible light networks, where each end is not meant to be mobile, and is not battery-free. Until recently, the idea of visible light passive communication has been introduced and exercised in [28, 41, 48]. Specifically, by using the incoming light from the existing indoor lighting infrastructure as the carrier, RetroVLC [28] uses the retroreflector fabric to backscatter the encoded information modulated by a LCD shutter and achieve 0.125 *kbps* using OOK modulation and Manchester coding[4]. PassiveVLC is built on the RetroVLC framework but achieves 1 *kbps* (8x over RetroVLC) using the same LCD shutter based on an optimized trend-based modulation and code-assisted demodulation design. The authors in [41] extends this idea by proposing a pixelated VLC backscatter, which uses multiple smaller reflectors and LCD shutters to form numbers of pixels and improves the link throughput proportionally from 200 *bps* to 600 *bps* by using three pixels. However, one potential limitation is that it only works when the communication distance is fixed. On the other hand, instead of modulating light sources, the author in [48] embed data as various grayscale seamless patterns into reflective surface objects. An optical receiver can leverage its relative mobility to the object to scan the time series of the photodiode sensor reading of the reflected optical pulse from the unmodulated ambient light signals to realize mobile data communication. PassiveVLC, by contrast, is able to dynamically changes the data to send on the reflecting link and thus is more suitable for IoT applications.

[4]This result is carried out by implementing RetroVLC on the same hardware as PassiveVLC. The LCD used in RetroVLC [28] has a significantly shorter response time and thus achieves 0.5 $kbps$.

Radio Backscatter Communication Systems. Backscattering is a way to provide transmission capability for extremely low-power devices, substituting the need for devices actively generating signals. The technique has been primarily used by RFID tags [20, 44]. Recently, TV-based [31, 36] and Wi-Fi [11, 22, 23, 49] systems started employing and advancing this technique. Our system shares the same design principles – achieve low energy communication by establishing a backscatter link. Although the current implementation of PassiveVLC is inferior to most radio backscatter system in terms of transmission rate (1 *kbps* versus several *kbps* [18, 22, 31, 46, 50] and even orders of *Mbps* [11, 23, 36, 49]) by a few orders of magnitude, our work has several advantages over RF-based approach in general: First, PassiveVLC is based on visible light, and thus completely immune to the interference from RF spectrum which is already crowded with "default" LAN and PAN technologies such as WiFi, BLE. Second, because of the backscattering nature, these RF-based systems tend to expose their transmissions to a wide surrounding area, leaving a good chance for side readers to overhear the information being transmitted. In contrast, ViTag relies on VLC, which implies that eavesdroppers are easily discernible. The use of retroreflectors further constraints the uplink transmission to stick along the tag-reader path. As a result, PassiveVLC comes with a good security property inherently, while other systems have to enhance their security with extra efforts [34, 51].

10 CONCLUSION

This paper present a first comprehensive attempt to the design, implementation, evaluation, demonstration and understanding of a practical backscattering communication system exploiting the visible light medium. With the proposed trend-based modulation and code-assisted demodulation design, we built a battery-free visible light backscatter tag and achieved up to 1 *kbps* uplink data rate, using commercially off-the-shelf retroreflector fabric and LCD shutter. While this technology is still in its infant stage, we believe this paper sheds light on new ways of thinking machine to machine communication in those scenarios where battery-free, sniff-proof, biologically friendly and spectral efficiency are much desired.

ACKNOWLEDGMENTS

We are grateful to the MobiCom reviewers for their constructive critique, and our shepherd, Dr. Yingying Chen in particular, for her valuable comments, all of which have helped us greatly improve this paper. We also thank Pan Hu, Liqun Li, Chao Sun, Xinyu Zhang, Chunshui Zhao and Lin Zhong for their thoughtful input and suggestions based on an early version of the work. This work is supported in part by National Key Research and Development Plan, China (Grant No. 2016YFB1001200), Science and Technology Innovation Project of Foshan City, China (Grant No. 2015IT100095) and Science and Technology Planning Project of Guangdong Province, China (Grant No. 2016B010108002).

REFERENCES

[1] [n. d.]. 3M Scotchlite 8906 Silver Fabric Trim. http://solutions.3m.com/wps/portal/3M/en_US/ScotchliteNA/Scotchlite/Products/~/8906-Silver-Fabric-Trim. ([n. d.]).

[2] [n. d.]. Basic Working Principle of LCD Panel. http://qxwujoey.tripod.com/lcd.htm. ([n. d.]).

[3] [n. d.]. DLP7000DLP®0.7 XGA 2x LVDS Type A DMD. http://www.ti.com/lit/ds/symlink/dlp7000.pdf. ([n. d.]).

[4] [n. d.]. Mobike. http://mobike.com/. ([n. d.]).

[5] [n. d.]. Monsoon power monitor. http://www.msoon.com/LabEquipment/PowerMonitor. ([n. d.]).

[6] Yuvraj Agarwal, Bharathan Balaji, Seemanta Dutta, Rajesh K Gupta, and Thomas Weng. 2011. Duty-cycling buildings aggressively: The next frontier in HVAC control. In *Proc. ACM/IEEE IPSN*.

[7] Alejandro Aragon-Zavala. 2008. *Antennas and propagation for wireless communication systems*. John Wiley & Sons.

[8] Harrison H Barrett and Stephen F Jacobs. 1979. Retroreflective arrays as approximate phase conjugators. *Optics letters* 4, 6 (1979).

[9] Ronen Basri and David W Jacobs. 2003. Lambertian reflectance and linear subspaces. *IEEE transactions on pattern analysis and machine intelligence* 25, 2 (2003).

[10] Donald J Berndt and James Clifford. 1994. Using dynamic time warping to find patterns in time series.. In *Proc. ACM KDD workshop*, Vol. 10.

[11] Dinesh Bharadia, Kiran Raj Joshi, Manikanta Kotaru, and Sachin Katti. 2015. Backfi: High throughput wifi backscatter. In *Proc. ACM SIGCOMM*.

[12] Trevor K Chan and Joseph E Ford. 2006. Retroreflecting optical modulator using an MEMS deformable micromirror array. *IEEE Journal of lightwave technology* 24, 1 (2006).

[13] CW Chow, CH Yeh, YF Liu, and Y Liu. 2011. Improved modulation speed of LED visible light communication system integrated to main electricity network. *Electronics letters* 47, 15 (2011).

[14] Kaiyun Cui, Gang Chen, Zhengyuan Xu, and Richard D Roberts. 2010. Line-of-sight visible light communication system design and demonstration. In *Proc. IEEE CSNDSP*.

[15] Biyi Fang, Nicholas D Lane, Mi Zhang, Aidan Boran, and Fahim Kawsar. 2016. BodyScan: Enabling radio-based sensing on wearable devices for contactless activity and vital sign monitoring. In *Proc. ACM MobiSys*.

[16] D. Giustiniano, N. O. Tippenhauer, and S. Mangold. 2012. Low-complexity visible light networking with led-to-led communication. In *IFIP Wireless Days*.

[17] John Frederick William Herschel. 1820. On the Rotation Impressed by Plates of Rock Crystal on the Planes of Polarization of the Rays of Light, as Connected with Certain Peculiarities in Its Crystallization. *Transactions of the Cambridge Philosophical Society* 1 (1820).

[18] Pan Hu, Pengyu Zhang, and Deepak Ganesan. 2015. Laissez-faire: Fully asymmetric backscatter communication. In *Proc. ACM SIGCOMM*.

[19] Colin Jenkins, J Gordon Brown, Lijie Li, Walter Johnstone, and Deepak Uttamchandani. 2007. MEMS retro-phase-modulator for free-space coherent optical communications. *IEEE Journal of Selected Topics in Quantum Electronics* 13, 2 (2007).

[20] S Jeon, Y Yu, and J Choi. 2006. Dual-band slot-coupled dipole antenna for 900 MHz and 2.45 GHz RFID tag application. *Electronics letters* 42, 22 (2006).

[21] Stephane Junique, Daniel Agren, Qin Wang, Susanne Almqvist, Bertrand Noharet, and Jan Y Andersson. 2006. A modulating retro-reflector for free-space optical communication. *IEEE photonics technology letters* 18, 1 (2006).

[22] Bryce Kellogg, Aaron Parks, Shyamnath Gollakota, Joshua R Smith, and David Wetherall. 2015. Wi-fi backscatter: internet connectivity for RF-powered devices. In *Proc. ACM SIGCOMM*.

[23] Bryce Kellogg, Vamsi Talla, Shyamnath Gollakota, and Joshua R Smith. 2016. Passive Wi-Fi: bringing low power to Wi-Fi transmissions. In *Proc. USENIX NSDI*.

[24] Toshihiko Komine and Masao Nakagawa. 2003. Integrated system of white LED visible-light communication and power-line communication. *IEEE Transactions on Consumer Electronics* 49, 1 (2003).

[25] Ye-Sheng Kuo, Pat Pannuto, Ko-Jen Hsiao, and Prabal Dutta. 2014. Luxapose: Indoor positioning with mobile phones and visible light. In *Proc. ACM MobiCom*.

[26] Hoa Le Minh, Dominic O'Brien, Grahame Faulkner, Lubin Zeng, Kyungwoo Lee, Daekwang Jung, YunJe Oh, and Eun Tae Won. 2009. 100-Mb/s NRZ visible light communications using a postequalized white LED. *IEEE Photonics Technology Letters* 21, 15 (2009).

[27] Hongdi Li, Yaqiang Liu, Tao Xing, Yu Wang, Jorge Uribe, Hossain Baghaei, Shuping Xie, Soonseok Kim, Rocio Ramirez, and Wai-Hoi Wong. 2003. An instantaneous photomultiplier gain calibration method for PET or gamma camera detectors using an LED network. In *IEEE Nuclear Science Symposium Conference Record*.

[28] Jiangtao Li, Angli Liu, Guobin Shen, Liqun Li, Chao Sun, and Feng Zhao. 2015. Retro-VLC: Enabling battery-free duplex visible light communication for mobile and iot applications. In *Proc. ACM HotMobile*.

[29] Liqun Li, Pan Hu, Chunyi Peng, Guobin Shen, and Feng Zhao. 2014. Epsilon: A visible light based positioning system. In *Proc. USENIX NSDI*.

[30] Tianxing Li, Chuankai An, Zhao Tian, Andrew T Campbell, and Xia Zhou. 2015. Human sensing using visible light communication. In *Proc. ACM MobiCom*.

[31] Vincent Liu, Aaron Parks, Vamsi Talla, Shyamnath Gollakota, David Wetherall, and Joshua R Smith. 2013. Ambient backscatter: wireless communication out of thin air. In *Proc. ACM SIGCOMM*.

[32] Jiakang Lu, Tamim Sookoor, Vijay Srinivasan, Ge Gao, Brian Holben, John Stankovic, Eric Field, and Kamin Whitehouse. 2010. The smart thermostat: using occupancy sensors to save energy in homes. In *Proc. ACM SenSys*.

[33] Changping Luo and KW Goossen. 2004. Optical microelectromechanical system array for free-space retrocommunication. *IEEE Photonics Technology Letters* 16, 9 (2004).

[34] Rajalakshmi Nandakumar, Krishna Kant Chintalapudi, Venkat Padmanabhan, and Ramarathnam Venkatesan. 2013. Dhwani: secure peer-to-peer acoustic NFC. In *Proc. ACM SIGCOMM*.

[35] Anh Nguyen, Raghda Alqurashi, Zohreh Raghebi, Farnoush Banaei-kashani, Ann C Halbower, and Tam Vu. 2016. A Lightweight And Inexpensive In-ear Sensing System For Automatic Whole-night Sleep Stage Monitoring. In *Proc. ACM SenSys*.

[36] Aaron N Parks, Angli Liu, Shyamnath Gollakota, and Joshua R Smith. 2014. Turbocharging ambient backscatter communication. In *Proc. ACM SIGCOMM*.

[37] G Goetz Peter, S Rabinovich William, Rita Mahon, L Murphy James, S Ferraro Mike, R Suite Michele, R Smith Walter, B Xu Ben, R Burris Harris, I Moore Christopher, et al. 2010. Modulating retro-reflector lasercom systems at the Naval Research Laboratory. In *Proc. IEEE Milcom*.

[38] William S Rabinovich, R Mahon, PG Goetz, E Waluschka, DS Katzer, SC Binari, and GC Gilbreath. 2003. A cat's eye multiple quantum-well modulating retroreflector. *IEEE Photonics Technology Letters* 15, 3 (2003).

[39] Niranjini Rajagopal, Patrick Lazik, and Anthony Rowe. 2014. Visual light landmarks for mobile devices. In *Proc. ACM/IEEE IPSN*.

[40] Stefan Schmid, Giorgio Corbellini, Stefan Mangold, and Thomas R Gross. 2013. LED-to-LED visible light communication networks. In *Proc. ACM MobiHoc*.

[41] Sihua Shao, Abdallah Khreishah, and Hany Elgala. 2016. Pixelated VLC-backscattering for Self-charging Indoor IoT Devices. *IEEE Photonics Technology Letters* (2016).

[42] Marc C Shults, Rathbun K Rhodes, Stuart J Updike, Barbara J Gilligan, and William N Reining. 1994. A telemetry-instrumentation system for monitoring multiple subcutaneously implanted glucose sensors. *IEEE Transactions on Biomedical Engineering* 41, 10 (1994).

[43] Zhao Tian, Kevin Wright, and Xia Zhou. 2016. The DarkLight rises: Visible light communication in the dark. In *Proc. ACM MobiCom*.

[44] Leena Ukkonen, Marijke Schaffrath, Daniel W Engels, L Sydanheimo, and Markku Kivikoski. 2006. Operability of folded microstrip patch-type tag antenna in the UHF RFID bands within 865-928 MHz. *IEEE Antennas and Wireless Propagation Letters* 5, 1 (2006).

[45] Jelena Vučić, Christoph Kottke, Stefan Nerreter, Klaus-Dieter Langer, and Joachim W Walewski. 2010. 513 Mbit/s visible light communications link based on DMT-modulation of a white LED. *IEEE Journal of lightwave technology* 28, 24 (2010).

[46] Anran Wang, Vikram Iyer, Vamsi Talla, Joshua R Smith, and Shyamnath Gollakota. 2017. FM Backscatter: Enabling Connected Cities and Smart Fabrics. In *Proc. USENIX NSDI*.

[47] Qing Wang, Domenico Giustiniano, and Daniele Puccinelli. 2014. OpenVLC: software-defined visible light embedded networks. In *Proc. ACM VLCS*.

[48] Qing Wang, Marco Zuniga, and Domenico Giustiniano. 2016. Passive Communication with Ambient Light. In *Proc. ACM CoNEXT*.

[49] Pengyu Zhang, Dinesh Bharadia, Kiran Joshi, and Sachin Katti. 2016. Hitchhike: Practical backscatter using commodity wifi. In *Proc. ACM SenSys*.

[50] Pengyu Zhang, Mohammad Rostami, Pan Hu, and Deepak Ganesan. 2016. Enabling practical backscatter communication for on-body sensors. In *Proc. ACM SIGCOMM*.

[51] Ruogu Zhou and Guoliang Xing. 2014. nShield: a noninvasive NFC security system for mobiledevices. In *Proc. ACM MobiSys*.

[52] Leah Ziph-Schatzberg, Thomas Bifano, Steven Cornelissen, Jason Stewart, and Zvi Bleier. 2009. Secure optical communication system utilizing deformable MEMS mirrors. In *Proc. SPIE*.